Investigating the role of N-terminal domain in phosphodiesterase 4B-inhibition by molecular dynamics simulation

Vidushi Sharma[1*], Sharad Wakode[1*]

[1]*Department of Pharmaceutical Chemistry, Delhi Institute of Pharmaceutical Sciences & Research, Mehrauli-Badarpur Road, Pushp vihar Sector 3 New Delhi 110017, India*

*Corresponding Author:

Vidushi Sharma

Email id: vidushimaitry@gmail.com

Contact no: +1-978-340-1547

Sharad Wakode

Email id: sharadwakode@gmail.com

Contact no: +91-9891008594

Keywords

Phosphodiesterase 4B, UCR2, Molecular dynamics simulation, Principal component analysis, Distance cross correlation matrix

Abstract

Phosphodiesterase 4B (PDE4B) is a potential therapeutic target for the inflammatory respiratory diseases such as congestive obstructive pulmonary disease (COPD) and asthma. The sequence identity of ~88% with its isoform PDE4D is the key barrier in developing selective PDE4B inhibitors which may help to overcome associated side effects. Despite high sequence identity, both isoform differs in few residues present in N-terminal (UCR2) and C-terminal (CR3) involved in catalytic site formation. Previously, we designed and tested specific PDE4B inhibitors considering N-terminal residues as a part of catalytic cavity. In continuation, current work thoroughly presents a MD simulation based analysis of N-terminal residues and their role in ligand binding. The various parameters viz. root mean square deviation (RMSD), radius of gyration (Rg), root mean square fluctuation (RMSF), principal component analysis (PCA), *dynamical cross-correlation matrix* (*DCCM*) analysis, secondary structure analysis, and residue interaction mapping were investigated to establish rational. Results showed enhanced ligand binding affinity in presence of N-terminal domain. Further, atomic level analysis indicated that T-pi and π-π interactions between inhibitors and residues are vital forces that regulate inhibitor association to PDE4B with high affinity. The derived information signifies potential of short range interactions in stabilizing PDE4B-inhibitor complexes, and may be helpful to design and evaluate next-generation selective PDE4B inhibitor.

1. Introduction

Respiratory inflammatory diseases such as congestive obstructive pulmonary disease (COPD) and asthma affect millions of people worldwide[1]. Phosphodiesterase 4B (PDE4B) is a potential therapeutic target in inflammatory diseases. It hydrolyses cyclic adenosine monophosphate (cAMP), an important secondary messenger, to 5'-adenosine monophosphates (AMP). AMP is a strong pro-inflammatory mediator in humans and thus PDE4B regulates many biological processes inside the cell by regulating the production of AMP[2]. Therefore, PDE4B inhibitors that prevent cAMP hydrolysis are much needed. The PDE4 enzyme family consists of four members (named PDE4A, PDE4B, PDE4C, and PDE4D) that are highly expressed in neutrophils, monocytes, central nervous system, and smooth muscles of the lung. Available non-selective PDE4 inhibitors like rolipram cause severe side effects such as nausea and emesis. As an improvement, the second-generation PDE4 inhibitors like roflumilast show less side effects, however are associated with narrow therapeutic window. Knockout studies in mice suggest that available PDE4B inhibitors co-inhibit PDE4D, a close homologous enzyme, thus causing
severe side effects[3],[4].Therefore, selective inhibition of PDE4B is much needed to develop safe anti-inflammatory drugs. Nonetheless, the high sequence (and thus structural) similarity between the two enzymes, PDE4B and PDE4D, sets hurdle to design and develop selective PDE4B inhibitors.

The structural comparison of the two enzymes, PDE4B and PDE4D, reveals that the active site cavity is composed of residues from the catalytic domain and from the upstream conserved region 2 (UCR2) domain[5]. While catalytic domain residues are conserved at the active site cavity between the two enzymes, the UCR2 domain shows following distinct residues that cover the active site region: PDE4B:PDE4D::Tyr274:Phe196[5]. Burgin *et al* have established that Tyr274 indeed provides selectivity for inhibition of PDE4B. Previously, we and other group have reported selective PDE4B inhibitors[6, 7]. Understanding the dynamics of UCR2-domain guided PDE4B inhibition will guide us to design and optimize available PDE4B inhibitors. Literature supports that similar MD simulation studies can successfully be implemented to understand the mechanisms of molecular recognition and conformational changes in therapeutic targets [8-15]. In this work, we performed a

comparative all-atom molecular dynamics simulation study of PDE4B-inhibitor complex and explored the effect of UCR2-domain residues in PDE4B inhibition. In 100ns long MD simulations, we performed principal component analysis (PCA), dynamical cross-correlation matrix (DCCM) analysis, secondary structure analysis, and residue network mapping to shed light on the fact that the N-terminal UCR2 domain improves non-polar interactions at PDE4B-inhibitor interface. Therefore, this UCR2 domain residues must be targeted to optimize PDE4B inhibitors[16, 17].

2. Experimental

2.1 Data selection

The highest resolution PDE4B crystal structure [PDB ID-2QYL inhibitor-NPV (4-[8-(3-nitrophenyl)-1,7-naphthyridin-6-yl] benzoic acid) resolution: 1.95 Å] was retrieved from the protein data[18]. To study the role of N-terminal UCR2 domain, we retrieved another PDE4B structure (PDB ID: 3G45, inhibitor: NPV, 8-(3-nitrophenyl)-6-(pyridin-4-ylmethyl)quinoline and resolution: 2.63 Å). Here onward, these complex structures will be denoted as "**U-Cat"** (structure with **U**CR2+**Cat**alytic domain; PDB ID: 3G45) and "**Cat"** (structure with only **cat**alytic domain; PDB ID: 2QYL). To understand the role of UCR-2 residues in PDE4B-inhibitor interactions, we used a common inhibitor, NPV, in both the structures and therefore replaced the coordinates of 988, a co-crystallized ligand, with NPV in the 3G45 structure.

2.2 Protein Preparation

Previously retrieved structures may have missing bond order, connectivity, steric clashes or bad contacts with the neighboring residues and therefore, both the structures were prepared using Protein Preparation Wizard (Impact 6.3, Schrodinger 2014-2, Maestro 9.8) [19] as previously described [15]. In brief, both the structures were corrected for atoms and bonds, and energy minimized to potentially relax the structures to get rid of any steric clashes in the structures.

2.3 Molecular Dynamic Simulations

FF14SB force field parameters were set for the protein using the AMBER14 (Assisted Model Building with Energy Refinement) LeaP module [20]. AM1-BCC method was used to assign partial atomic charges for bound inhibitor (NPV) and general amber force field (GAFF) was used to create its topology [21]. Mg^{2+} and Zn^{2+} ions were

115 treated according to the “non-bonded” model method [22]. The prepared systems were
116 solvated with TIP3P water model by creating an cubic water box, where distance of
117 the box was set to 10Å from periphery of protein [23]. Molecular systems were
118 neutralized through the AMBER LeaP module by the addition of necessary amount of
119 counter ions (Na^+) to construct the system in electrostatically preferred position.

120 The whole assembly was then saved as the prepared topology and coordinate files to
121 use as input for the PMEMD module of the AMBER [24]. At the first step, the prepared
122 systems were energy minimized in a two step process: initial 1000 steps of steepest
123 descent followed by 500 steps conjugate gradient. In the first part of minimization, the
124 complex was kept fixed to allow water and ion molecules to move, followed by the
125 minimization of the whole system (water, ions and complex) in the second part. The
126 minimized systems were gradually heated from 0 to 298 K using a NVT ensemble for
127 100ps where the protein-ligand complex was restrained with a large force constant of
128 5 kcal/mol/$Å^2$. Following heating, the systems were equilibrated under constant
129 pressure at 298 K and the restrain was gradually removed at NPT ensemble as
130 follows: 5 kcal/mol/$Å^2$ (40 ps), 2 kcal/mol/$Å^2$ (20 ps), 1 kcal/mol/$Å^2$ (20 ps) and 0.5 k
131 cal/mol/$Å^2$ (10 ps). Final simulations, the production run, were performed for 100 ns on
132 NPT ensemble at 298 K temperature and 1 atm pressure. The step size of 2 fs was
133 kept for whole simulation study. Langev in thermostat and barostat were used for
134 temperature and pressure coupling. SHAKE algorithm was applied to constrain all
135 bonds containing hydrogen atoms [25]. Non-bonded cutoff was kept on 10Å and long
136 range electrostatic interactions were treated by Particle Mesh Ewald method (PME)
137 with fast Fourier transform grid spacing of approximately 0.1nm [26]. Trajectory
138 snapshots were taken at each 100ps, which were used for final analysis. The
139 minimization and equilibration were performed by PMEMD module of AMBER14. The
140 production simulations were performed using PMEMD program of AMBER running on
141 NVIDIA Tesla C2050 GPU work station [27]. The production run was considered for
142 the analysis which was carried out using the cpptraj module of the AMBER14 and
143 VMD [28]

144 **2.4 Root-mean-square deviation (RMSD)**

145 The stability of the two systems during the simulations was studied by calculating the
146 root-mean-square deviation (RMSD) of the backbone atoms of different frames to the
147 initial conformation (RMSD) and therefore RMSD is the measure of the average

distance between the atoms (usually the backbone atoms) of superimposed protein structures. RMSD of Cα atoms was calculated using the cpptraj analysis tool in the AMBER program. The equation below illustrates the RMSD:

$$\textbf{RMSD} = \frac{1}{N}\sum_{i}^{N} \delta_i^2$$

where δ is the distance between N pairs of equivalent atoms.

2.5 Radius of Gyration (Rg)

Radius of gyration is a measure of the distance between the centre of mass and both termini of the protein and therefore radius of gyration determines the compactness of protein structure [29]. The average Rg was computed by taking the average over at least 5000 frames of the trajectory.

2.6 Relative mean square fluctuation (RMSF)

To study the effect of UCR2-domain residues on the overall protein flexibility, average fluctuation values were followed for individual amino acid residues during the simulations. The RMSFs were calculated with the backbone atoms of amino acid residues for both the structures using the following formula:

$$RMSF_{(v)} = \sqrt{\frac{1}{T}\sum_{t=1}^{T}(v_t - \bar{v})^2} \qquad \text{T= number of frames}$$

RMSF values were calculated using the cpptraj module of AMBER 14.

2.7 Dynamics cross correlation matrix

The dynamic profile of the protein in the simulations can be analyzed to produce information of the correlated motions. Correlated motions can occur between regions such as domain–domain communication and proximal residues. In the present work, the cross correlation of the atomic fluctuations was examined which was obtained from the simulations. The cross correlation was calculated as block average over time from 50 ns to 100 ns from the MD trajectories. We use the first coordinate set of the analysis portion of the simulation, *i.e.,* starting structure, as a reference set. Each subsequent coordinate set was translated and then rotated to obtain the minimum rms deviation of the Cα atoms from the reference coordinate set [30].

The analysis is based upon the formula:

$$C(i,j) = \frac{c(i,j)}{c(i,i)^{\frac{1}{2}} \,.\, c(j,j)^{\frac{1}{2}}}$$

where *c(i,j)* is the covariance matrix element of protein fluctuation between residues *i* and *j.*

2.8 Principle component analysis (PCA)

Principal component analysis (PCA) is a statistical technique to find out patterns in high-dimensional data. Very often it is used as a tool in exploratory data analysis which aid in divulge the internal data structure in best way of explaining its variance. PCA if performed on a group of experimental structures or MD trajectory, the PCs can highlight major conformational changes between the structures and describe concerted atomic displacements [31]. These motions are mostly essential for protein function, the dynamics in this low-dimensional subspace spanned by the first few PCs is termed “essential dynamics”. For our study, we performed this exercise to monitor the effect of UCR2-domain residues on the dynamics of the catalytic domain of PDE4B. Mathematically, the PCs are obtained by a diagonalization of the data covariance (or correlation) matrix C. The covariance matrix C of the atomic coordinates is constructed as follows:

$$\mathbf{C = V\Lambda V^T}$$

Where the results in the diagonal matrix Λ contains the eigenvalues as diagonal entries and the matrix V contains the corresponding eigenvector.

2.9 Protein secondary structure analysis

In the dynamic analysis, it is imperative to identify critical changes in secondary structure element during simulation. It imparts deep insight into the stability of the secondary structure. Each secondary structure type is shown by different colour and a change in secondary structure type is easily differentiated. The secondary structure information for each frame was calculated and a two-dimensional plot was generated for last 50 ns trajectory, 500 frames.

2.10 Residue network mapping

The study of residue interacting pattern is imperative to analyse protein's structural rigidity, secondary structure maintenance and functionality. It includes the crucial interaction, hydrogen bonds occupancy that are present during the simulation. These interactions are identified using VMD. The hydrogen bond interaction was calculated between the polar hydrogen atom and a nearby (< 3.4 Å) acceptor atom. Similarly, the π -π interactions were calculated in crystal structure and MD-simulated structure of the last 100th ns. The π -π interactions results with attraction of one π electron cloud system with another nearby π electron cloud system. These interactions are crucial in bioprocesses. In this study, we measure the inter-residue distance to each hydrophobic ring centroid to identify the pair of π -π interacting residues. The residue pairs within a ring centroid distance of 3.0–7.5 Å (min-max) were considered. Further, we calculated the dihedral angle (θ) between the two planes that have two types of structural geometries. If the geometrical angle between the planes of two rings was found to be 30° > θ > 150°, the rings are in face-to-face interaction and if the angle is between 30° < θ < 150°, the rings are in in T-shaped (edge to face or perpendicular) interactions [32] .

3. Result and discussion

The objective of our study was to understand the role of N-terminal UCR2-domain residues in the stability of PDE4B-inhibitor complexes. To this end, we performed all atom molecular dynamics simulations of PDE4B-NPN complex in the presence (**U-Cat**) and absence of the UCR2-domain residues (**Cat**). First we confirmed the stability of two systems by the root mean square deviation (RMSD) analysis and total energy calculations. Next, the stable MD trajectories were processed to understand the dynamics of PDE4B-NPV interactions through the root mean square fluctuation (RMSF) analysis, the dynamical cross-correlation matrix (DCCM) analysis and the principle component analysis (PCA). Lastly, we analyzed residue network mapping.

3.1 Systems stability

The reliability of our MD simulations was assessed in terms of the root mean square deviations (RMSD) values, total energies and radius of gyration (Rg) of the two simulations as follows:

3.1.1 Root mean square deviations (RMSD)

241 The root mean-square deviation (RMSD) analysis accounts for the average distance
242 between the selected atoms of superimposed biomolecules which indicates the
243 closeness between the three-dimensional structures. In this study, we calculated the
244 RMSD values for the backbone atoms for the proteins and for all non-hydrogen atoms
245 for the small molecule, NPV. Within initial 5-ns of each simulations, both the systems
246 became stable and remained stable throughout the 100ns long MD simulations **(Fig.**
247 **1)**. During last 50 ns long simulations, the RMSD values of catalytic domain residues
248 (Ser324-Pro665) were as follows: 1.28 ± 0.12 Å (**Cat**) and 1.11 ± 0.09 Å (**U-Cat**). The
249 lower magnitude of these values suggests the stability of both the systems. Further
250 the difference between these values for both the systems (**U-Cat** versus **Cat**
251 complexes) is insignificant (t-test) suggesting that the additional N-terminal, UCR2-
252 domain does not affect the major dynamics of catalytic domain of the protein.

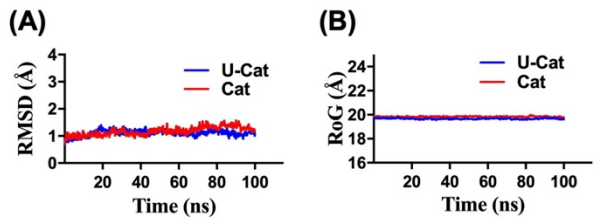

Figure 1: RMSD and RoG plots of two complexes.

253

254 Similar to RMSD values for catalytic domain, the RMSD values for the bound inhibitor,
255 NPV, are also low (<1.5 Å) suggesting the stable dynamics of the two systems. The
256 RMSD values for the two systems during last 50 ns duration are as follows: 1.16±0.07
257 Å (**Cat**) and 0.86±0.26 Å (**U-Cat**). The lower RMSD values for **U-Cat** system suggest
258 that additional UCR2-domain stabilizes the bound inhibitor.

259

260 ***3.1.2 Radius of gyration***

261 The radius of gyration (Rg) measures the mass-weighted RMS distance of a group of
262 atoms from their common centre of mass which indicates dimension of the protein
263 globally. For both the systems (**Cat** and **U-Cat**), we calculated the Rg for the catalytic
264 domain residues (Ser324-Pro658) and observed a stable trend in Rg plot. The RoG
265 values for the last 50 ns simulations for the two systems were as follows: 19.66±0.05
266 (**Cat** system) and 19.78 ± 0.05 (**U-Cat** system) (**Fig. 1B**).

267

268 **3.2 Structural dynamics of PDE4B-NPN complex in presence (U-Cat) and**
269 **absence (Cat) of UCR2-domain**
270 Once we confirmed the stability of the two systems, next we sought to study the
271 conformational changes in the two complexes (**Cat** and **U-Cat**) and performed
272 following analyses:
273
274 ***3.2.1 Root mean square fluctuation***
275 To understand and compare the dynamics of the two complexes, we calculated the
276 root mean square fluctuation (RMSF) values for each complex. Using RMSF analysis,
277 we studied the fluctuation at the individual residue level in the two systems. In order
278 to compare the two systems, we rejected the additional N-terminal residues in **U-Cat**
279 structure and focussed at the catalytic domain residues in the two complex structures.
280 The comparative RMSF plot of the two systems is shown in **Fig. 2**. A similar trend in
281 RMSF values suggested that the UCR2-domain had no drastic effect on the
282 conformational dynamics of the two systems.
283

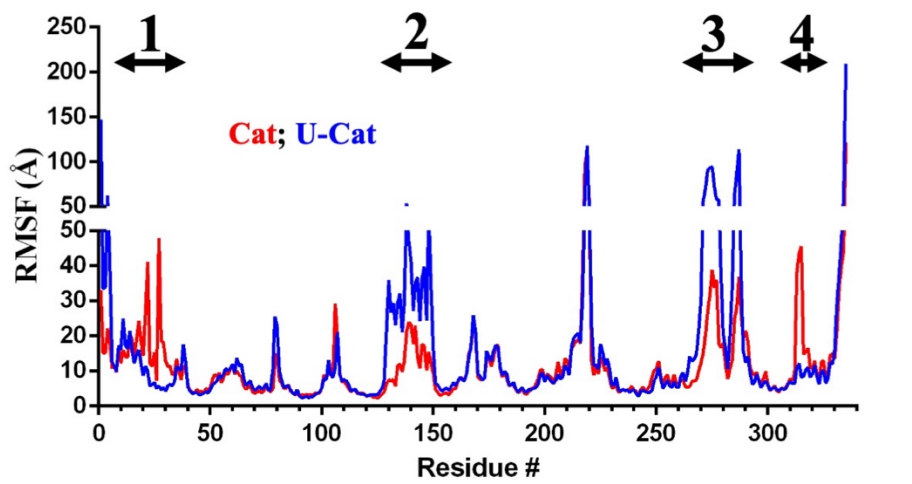

Figure 2: RMSF plot of the two complexes.

284
285 Intriguingly, we observed the distinct behaviours of the two complexes, **U-Cat** and **Cat**,
286 in following four regions: Asp336-Asn354 (**region I**; 19 residues), Pro451-Glu472
287 (**region II**; 22 residues), Phe587-Ser614 (**region III**; 28 residues) and Gln635-Asp643
288 (**region IV**; 13 residues). Among these regions, the presence of additional UCR2-
289 domain residues stabilized the **region I** and **IV** in **U-Cat** complex, that reflects in the
290 lower RMSF values as compared to **Cat** complex. In contrast, **region II** and **III** showed

291 higher RMSF values for the **U-Cat** complex. Based on the locations of these four
292 regions with respect to **UCR2-domain**, we hypothesized that UCR2-domain may
293 affect the correlative motion of the catalytic domain of PDE4B and sought to perform
294 the dynamical cross-correlation matrix analysis.
295
296 ***3.2.2 Dynamical cross-correlation matrix (DCCM)***
297 To understand the variation in the RMSF values of the two complexes and to check if
298 motions in different regions (**I-IV**) are correlated or not, we performed an inter-residue
299 dynamical cross-correlation matrix (DCCM) analysis for Cα atoms to find out the extent
300 of correlation of atomic movements (**Fig. 3**).

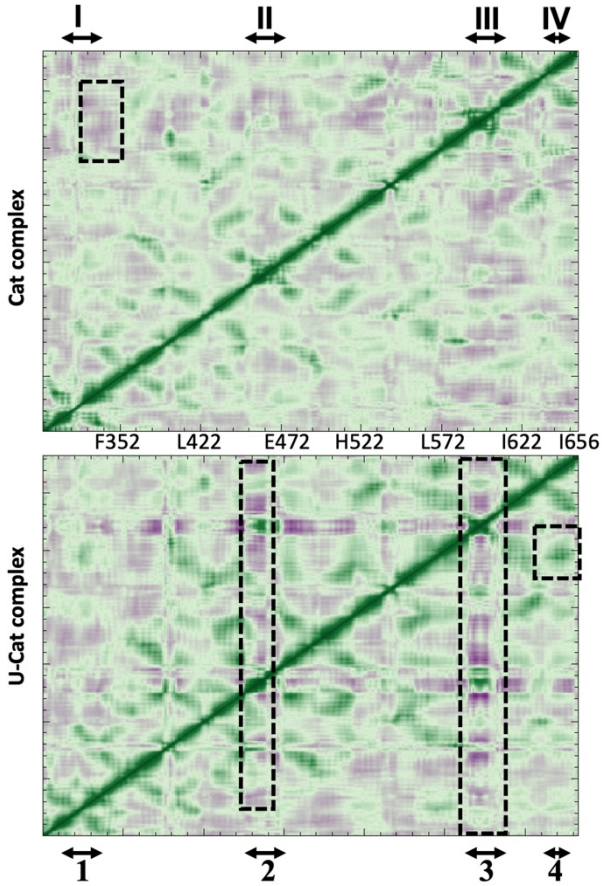

Figure 3: Dynamic Cross Correlation Map (DCCM) maps of the two complexes.

301
302 To compare the two complex structures, **U-Cat** and **Cat**, we only considered the
303 catalytic (**Cat**) residues in the two complexes to perform the DCCM analysis. Similar
304 diagonal trends in the two figures suggested that the UCR2-domain had severe effect
305 on the **secondary structure** of the two complexes suggesting that the two systems,
306 **U-Cat** and **Cat**, may have similar global dynamics. Further, the darker shades of

307 colours in **U-Cat** complex suggested that the presence of additional UCR2-domain
308 caused a higher extent of correlative (green) and anticorrelative (purple) motions in
309 PDE4B-NPV complex. In particular, we observed intense purple shades in **region II**
310 and **III** of **U-Cat** complex suggesting a stronger anti-correlative motions in these region.
311 Intriguingly, these anti-correlative motions in region II and III were correlated with the
312 high RMSF values in the regions (**Fig. 2 and 3**). On the contrary, **region I and IV**
313 showed enhanced correlative motion in presence of UCR2-domain in the **U-Cat**
314 complex. The darker green shades plausibly represent the stability in these regions
315 which is further supported by decrease RMSF values in these two regions (**Fig. 2 and**
316 **3**).
317
318 ***3.2.3 Principle component analysis (PCA)***
319 In the DCCM study, we confirmed that the presence of UCR2-domain indeed affected
320 the correlative (and anti-correlative) motions in PDE4B-NPV complex. To understand
321 the directionality of these motions, we proceeded further and performed a PCA of the
322 two simulations (**U-Cat** and **Cat**). Here, we designated the whole average of receptor
323 motion based on Cα atoms. This approach supported to figure out the overall
324 combined motion of the Cα atoms in the protein denoted by the eigenvectors of the
325 covariance matrix which is asserted by its coincident eigenvalues [31]. The occurrence
326 of the eigenvectors associated with large eigenvalues can generally represent the
327 over-all concerted motion of the protein correlated to the protein function. The
328 increasing sum of eigenvalues as a function of number of eigenvalues resulting from
329 the MD simulation frames during 0.1μs is shown in **(Fig. 4A)**. To compare the two
330 complexes, we ruled out additional residues of UCR2-domain in **U-Cat**. We observed
331 that the first two components of the analysis, PC1 and PC2 were significantly higher
332 for the **U-Cat** complex as compared to the **Cat** complex suggesting that the additional
333 UCR2-domain indeed enhances the directional motion at the catalytic domain of
334 PDE4B. **Fig. 4B** shows the domains, directions and degrees of motions corresponding
335 to the first three PCs of each complex. We found that PC1 and PC2 motions confined
336 to regions Phe587-Ser610 and Asp447-Asp472 in the **U-Cat** structure. Intriguingly,
337 these two regions corresponds to region II and III of RMSF plot (**Fig. 2**) and DCCM
338 (**Fig. 3**) and thus link with the anticorrelative motion in the protein.
339 Taken together, our RMSF, DCCM and PCA results suggested that the presence of
340 UCR2-domain affected the dynamics of the catalytic domain of PDE4B. Interestingly,

region II and III that showed anticorrelative motions and large RMSF values were distant from the active site region. On the contrary, region I and IV that showed correlative motion and lower RMSF values, included the active site residues. Therefore, the additional domain UCR2-domain enhanced the correlative motion at the active site cavity and thus stabilized the protein-inhibitor interactions.

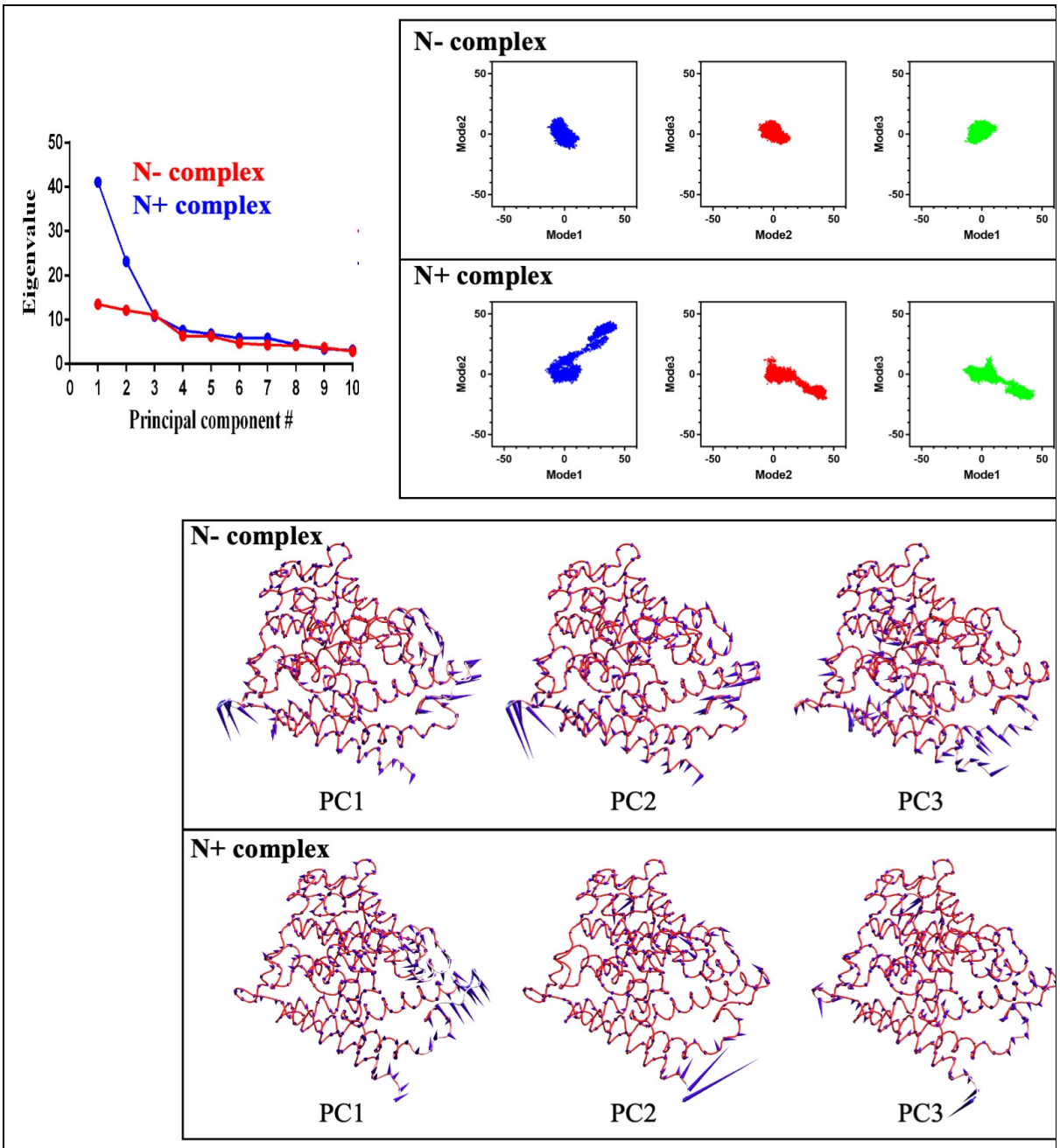

Figure 4. Principle component analysis of the two complexes. Top(left): Plot of first ten-principle components (PCs). Top (right): Plot of first three-PCs. Bottom: Porcupine plots of first 3-PCs of the two complexes.

348 ***3.2.4 Secondary structure analysis***

349 Further, to visualize critical changes in the protein conformation during the timeline
350 analysis, we performed a secondary structure analysis of the two simulations. We
351 generated a two-dimensional plot secondary structure information for the 100ns
352 trajectory (**Fig. 5**). We observed that region Ser423-Asp433, which was a turn in the
353 **U-Cat** complex, changed to a 3-turn helix in the **Cat** complex (brown to green). Further,
354 we observed a local structural transition at the region Glu343–Phe353 that was a turn
355 in the **Cat** complex but transformed into a coil in the presence of the UCR2-domain in
356 the **U-Cat** complex, shown as green to red transition in **Fig. 5**. We observed a similar
357 transition at the region Thr535-Thr550 that turned from a coil in the **Cat** complex to an
358 anti-parallel beta-sheet in **U-Cat** complex as seen a transition from red to blue colour
359 in the **Fig. 5**. Intriguingly, these differences in the secondary structure were in
360 agreement with the RMSF and DCCM analyses and thus suggested the flexible
361 residues.

362

363 **3.3 The dynamics of the active site region**

364 To further understand the effect of additional UCR2-domain on the catalytic domain of
365 PDE4B, we studied the dynamics of the active site region in detail. At first, we
366 assessed the stability of an H-bond with Gln615, an interaction reported in the crystal
367 structure. We observed a stable H-bond with Gln615 in both the simulations, **U-Cat**
368 and **Cat** complexes. Further, we observed an enhanced occupancy of 65% of Gln615-
369 Hbond in **U-Cat** complex in comparison to 43% observed in **Cat** complex suggesting
370 that the additional UCR2-domain indeed stabilizes the PDE4B-inhibitor interactions.
371 Furthermore, we observed an additional H-bond with Tyr274 (occupancy 25%) in **U-**
372 **Cat** complex which was otherwise absent in the simulation of the Cat complex. Next,
373 we studied the dynamics of the other plausible H-bonding residues in the active site
374 cavity [6]. These residues include Tyr274, Tyr405, His406, His410, Tyr415, Asp447,
375 Asp564, Asn567 and Gln615. We observed that these plausible H-bonding residues
376 were more stable in the **U-Cat** complex as compared to **Cat** complex as interpreted
377 by lower RMSD values.
378 In addition to H-bonding residues, π-π interactions with Phe618, Phe586, Tyr405 and
379 Tyr274 were stable and consistent with the interactions reported in the crystal
380 structures (**Fig. 6**).

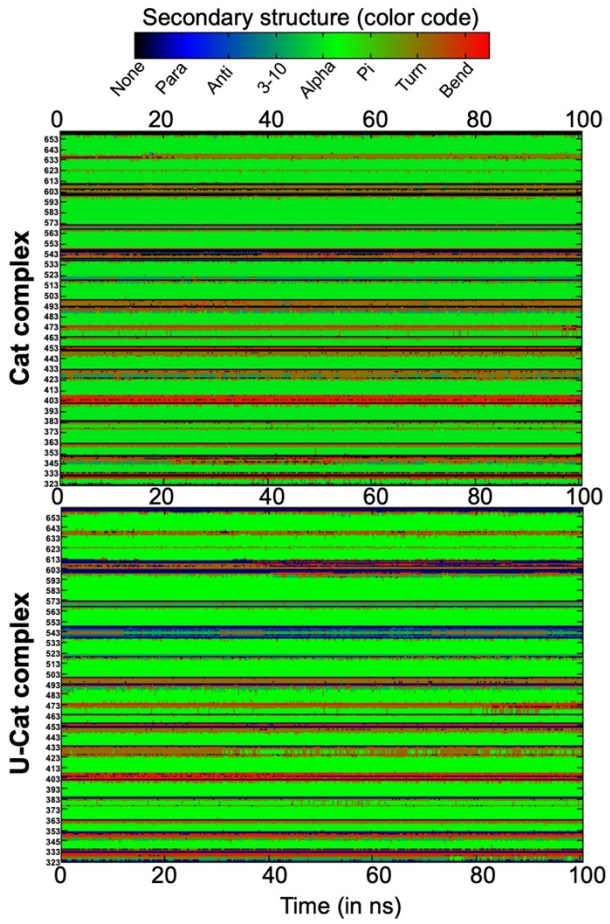

Figure 5. Secondary structure plot of the two complexes during 100 ng long simulations.

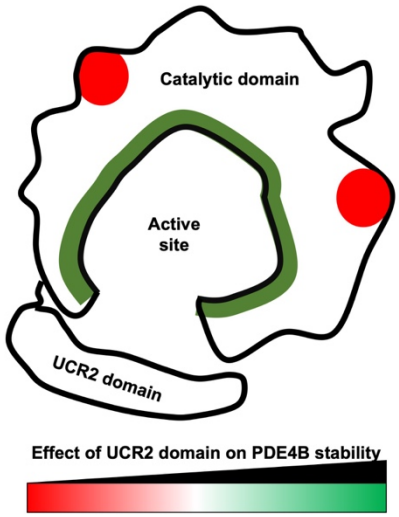

Figure 6. An illustration to show the effect of additional UCR2 domain residues on the stability of the catalytic domain.

Altogether, our simulations and post-trajectory analyses confirm that the additional UCR2-domain stabilizes the PDE4B-inhibitor complexes and therefore must be considered while evaluating the binding stability of newly designed PDE4B inhibitors.

4. Conclusion

We performed 100 ns long molecular dynamics simulations of PDE4B variants, with and without the UCR2-domain, both complexes with a common inhibitor, NPV, and probed the effect of additional UCR2-domain on the stability of PDE4B-NPV interactions. RMSF, DCCM, PCA, H-bond network analyses confirm that the UCR2-domain enhances the correlation and anticorrelation motion in the complex structure. This study provides substantial evidence to include the regulatory UCR2-domain in further drug designing to evaluate the stability of newly designed PDE4B inhibitors.

.

References

1. Zhang KY, Ibrahim PN, Gillette S, Bollag G. Phosphodiesterase-4 as a potential drug target. Expert Opinion on Therapeutic Targets. 2005. doi: 10.1517/14728222.9.6.1283.
2. Houslay MD, Adams DR. PDE4 cAMP phosphodiesterases: modular enzymes that orchestrate signalling cross-talk, desensitization and compartmentalization. Biochem J. 2003;370(Pt 1):1-18. Epub 2002/11/26. doi: 10.1042/bj20021698. PubMed PMID: 12444918; PubMed Central PMCID: PMCPMC1223165.
3. Calverley PM, Rabe KF, Goehring UM, Kristiansen S, Fabbri LM, Martinez FJ. Roflumilast in symptomatic chronic obstructive pulmonary disease: two randomised clinical trials. Lancet. 2009;374(9691):685-94. Epub 2009/09/01. doi: 10.1016/s0140-6736(09)61255-1. PubMed PMID: 19716960.
4. Wang P, Myers JG, Wu P, Cheewatrakoolpong B, Egan RW, Billah MM. Expression, purification, and characterization of human cAMP-specific phosphodiesterase (PDE4) subtypes A, B, C, and D. Biochem Biophys Res Commun. 1997;234(2):320-4. Epub 1997/05/19. doi: 10.1006/bbrc.1997.6636. PubMed PMID: 9177268.
5. Rocque WJ, Tian G, Wiseman JS, Holmes WD, Zajac-Thompson I, Willard DH, et al. Human recombinant phosphodiesterase 4B2B binds (R)-rolipram at a single site with two affinities. Biochemistry. 1997;36(46):14250-61. Epub 1997/12/31. doi: 10.1021/bi971112e. PubMed PMID: 9369498.
6. Sharma V, Wakode S. Structural insight into selective phosphodiesterase 4B inhibitors: pharmacophore-based virtual screening, docking, and molecular dynamics simulations. J Biomol Struct Dyn. 2017;35(6):1339-49. Epub 2016/05/04. doi: 10.1080/07391102.2016.1183520. PubMed PMID: 27136969.
7. Goto T, Shiina A, Murata T, Tomii M, Yamazaki T, Yoshida K, et al. Identification of the 5,5-dioxo-7,8-dihydro-6H-thiopyrano[3,2-d]pyrimidine derivatives as highly selective PDE4B inhibitors. Bioorg Med Chem Lett. 2014;24(3):893-9. Epub 2014/01/15. doi: 10.1016/j.bmcl.2013.12.076. PubMed PMID: 24412069.
8. Padhi AK, Kumar H, Vasaikar SV, Jayaram B, Gomes J. Mechanisms of loss of functions of human angiogenin variants implicated in amyotrophic lateral sclerosis. PLoS One. 2012;7(2):e32479. Epub 2012/03/03. doi: 10.1371/journal.pone.0032479. PubMed PMID: 22384259; PubMed Central PMCID: PMCPMC3288110.
9. Moreau CA, Bhargav SP, Kumar H, Quadt KA, Piirainen H, Strauss L, et al. A unique profilin-actin interface is important for malaria parasite motility. PLoS Pathog. 2017;13(5):e1006412. Epub 2017/05/30. doi: 10.1371/journal.ppat.1006412. PubMed PMID: 28552953; PubMed Central PMCID: PMCPMC5464670.
10. Santos JM, Egarter S, Zuzarte-Luis V, Kumar H, Moreau CA, Kehrer J, et al. Malaria parasite LIMP protein regulates sporozoite gliding motility and infectivity in mosquito and mammalian hosts. Elife. 2017;6. Epub 2017/05/20. doi: 10.7554/eLife.24109. PubMed PMID: 28525314; PubMed Central PMCID: PMCPMC5438254.
11. Douglas RG, Nandekar P, Aktories JE, Kumar H, Weber R, Sattler JM, et al. Inter-subunit interactions drive divergent dynamics in mammalian and Plasmodium actin filaments. PLoS Biol. 2018;16(7):e2005345. Epub 2018/07/17. doi: 10.1371/journal.pbio.2005345. PubMed PMID: 30011270; PubMed Central PMCID: PMCPMC6055528.
12. Kumar D, Kumari K, Jayaraj A, Kumar V, Kumar RV, Dass SK, et al. Understanding the binding affinity of noscapines with protease of SARS-CoV-2 for COVID-19 using MD simulations at different temperatures. J Biomol Struct Dyn. 2020:1-14. Epub 2020/05/05. doi: 10.1080/07391102.2020.1752310. PubMed PMID: 32362235.

13. Islam R, Parves R, Paul AS, Uddin N, Rahman MS, Mamun AA, et al. A Molecular Modeling Approach to Identify Effective Antiviral Phytochemicals against the Main Protease of SARS-CoV-2. J Biomol Struct Dyn. 2020:1-20. Epub 2020/04/29. doi: 10.1080/07391102.2020.1761883. PubMed PMID: 32340562.
14. Elfiky AA. SARS-CoV-2 RNA dependent RNA polymerase (RdRp) targeting: an in silico perspective. J Biomol Struct Dyn. 2020:1-9. Epub 2020/04/28. doi: 10.1080/07391102.2020.1761882. PubMed PMID: 32338164.
15. Sharma V, Wakode S. Pharmacophore generation and atom based 3D-QSAR of quinoline derivatives as selective phosphodiesterase 4B inhibitors. RSC Advances. 2016;6(79):75805-19. doi: 10.1039/C6RA11210B.
16. Xiao F, Yang M, Xu Y, Vongsangnak W. Comparisons of Prostate Cancer Inhibitors Abiraterone and TOK-001 Binding with CYP17A1 through Molecular Dynamics. Comput Struct Biotechnol J. 2015;13:520-7. Epub 2015/12/19. doi: 10.1016/j.csbj.2015.10.001. PubMed PMID: 26682016; PubMed Central PMCID: PMCPMC4652021.
17. Tautermann CS, Seeliger D, Kriegl JM. What can we learn from molecular dynamics simulations for GPCR drug design? Comput Struct Biotechnol J. 2015;13:111-21. Epub 2015/02/25. doi: 10.1016/j.csbj.2014.12.002. PubMed PMID: 25709761; PubMed Central PMCID: PMCPMC4334948.
18. Berman HM, Westbrook J, Feng Z, Gilliland G, Bhat TN, Weissig H, et al. The protein data bank. Nucleic acids research. 2000;28(1):235-42.
19. Sastry GM, Adzhigirey M, Day T, Annabhimoju R, Sherman W. Protein and ligand preparation: parameters, protocols, and influence on virtual screening enrichments. J Comput Aided Mol Des. 2013;27(3):221-34. Epub 2013/04/13. doi: 10.1007/s10822-013-9644-8. PubMed PMID: 23579614.
20. Hornak V, Abel R, Okur A, Strockbine B, Roitberg A, Simmerling C. Comparison of multiple Amber force fields and development of improved protein backbone parameters. Proteins. 2006;65(3):712-25. Epub 2006/09/19. doi: 10.1002/prot.21123. PubMed PMID: 16981200; PubMed Central PMCID: PMCPMC4805110.
21. Wang J, Wolf RM, Caldwell JW, Kollman PA, Case DA. Development and testing of a general amber force field. J Comput Chem. 2004;25(9):1157-74. Epub 2004/04/30. doi: 10.1002/jcc.20035. PubMed PMID: 15116359.
22. Stote RH, Karplus M. Zinc binding in proteins and solution: a simple but accurate nonbonded representation. Proteins. 1995;23(1):12-31. Epub 1995/09/01. doi: 10.1002/prot.340230104. PubMed PMID: 8539245.
23. Kiss PT, Baranyai A. Sources of the deficiencies in the popular SPC/E and TIP3P models of water. J Chem Phys. 2011;134(5):054106. Epub 2011/02/10. doi: 10.1063/1.3548869. PubMed PMID: 21303091.
24. Case DA, Cheatham TE, 3rd, Darden T, Gohlke H, Luo R, Merz KM, Jr., et al. The Amber biomolecular simulation programs. J Comput Chem. 2005;26(16):1668-88. Epub 2005/10/04. doi: 10.1002/jcc.20290. PubMed PMID: 16200636; PubMed Central PMCID: PMCPMC1989667.
25. Gunsteren WFv, Berendsen HJC. Algorithms for macromolecular dynamics and constraint dynamics. http://dxdoiorg/101080/00268977700102571. 2006. doi: Molecular Physics, Vol. 34, No. 5, 1311–1327, November 1977.
26. Darden T, York D, Pedersen L. Particle mesh Ewald: An N·log(N) method for Ewald sums in large systems. 1993. doi: 1.464397.
27. Gotz AW, Williamson MJ, Xu D, Poole D, Le Grand S, Walker RC. Routine Microsecond Molecular Dynamics Simulations with AMBER on GPUs. 1. Generalized Born. J Chem Theory Comput. 2012;8(5):1542-55. Epub 2012/05/15. doi: 10.1021/ct200909j. PubMed PMID: 22582031; PubMed Central PMCID: PMCPMC3348677.

28. Humphrey W, Dalke A, Schulten K. VMD: visual molecular dynamics. J Mol Graph. 1996;14(1):33-8, 27-8. Epub 1996/02/01. PubMed PMID: 8744570.
29. Lobanov M, Bogatyreva NS, Galzitskaia OV. [Radius of gyration is indicator of compactness of protein structure]. Mol Biol (Mosk). 2008;42(4):701-6. Epub 2008/10/17. PubMed PMID: 18856071.
30. McCammon AJ, Harvey SC. Dynamics of Proteins and Nucleic Acids. Cambridge University Press1988.
31. Amadei A, Linssen AB, Berendsen HJ. Essential dynamics of proteins. Proteins. 1993;17(4):412-25. Epub 1993/12/01. doi: 10.1002/prot.340170408. PubMed PMID: 8108382.
32. Anjana R, Vaishnavi MK, Sherlin D, Kumar SP, Naveen K, Kanth PS, et al. Aromatic-aromatic interactions in structures of proteins and protein-DNA complexes: a study based on orientation and distance. Bioinformation. 2012;8(24):1220-4. Epub 2013/01/01. doi: 10.6026/97320630081220. PubMed PMID: 23275723; PubMed Central PMCID: PMCPMC3530875.